Available online at www.sciencedirect.com

jmr&t Journal of Materials Research and Technology

journal homepage: www.elsevier.com/locate/jmrt

Original Article

Characterization of compressed bacterial cellulose nanopaper film after exposure to dry and humid conditions

Hairul Abral [a,*], *Melati Krista Chairani* [a], *Muhammad Dinul Rizki* [a], *Melbi Mahardika* [e], *Dian Handayani* [b], *Eni Sugiarti* [c], *Ahmad Novi Muslimin* [c], *S.M. Sapuan* [d], *R.A. Ilyas* [f]

[a] *Department of Mechanical Engineering, Andalas University, 25163 Padang, Sumatera Barat, Indonesia*
[b] *Laboratory of Sumatran Biota, Faculty of Pharmacy, Andalas University, 25163 Padang, Sumatera Barat, Indonesia*
[c] *Laboratory of High-Temperature Coating, Research Center for Physics Indonesian Institute of Sciences (LIPI) Serpong, Indonesia*
[d] *Department of Mechanical and Manufacturing Engineering, Faculty of Engineering, Universiti Putra Malaysia, 43400 UPM Serdang, Selangor, Malaysia*
[e] *Department of Biosystems Engineering, Institut Teknologi Sumatera, 35365 South Lampung, Indonesia*
[f] *School of Chemical and Energy Engineering, Faculty of Engineering, Universiti Teknologi Malaysia, 81310 Skudai, Johor Bahru, Johor, Malaysia*

ARTICLE INFO

Article history:
Received 25 September 2020
Accepted 15 January 2021
Available online 27 January 2021

Keywords:
Lattice strain
Bacterial cellulose
Nanofiber
Relaxation
Residual stress

ABSTRACT

This work investigates the effects of two different levels of humidity (RH 50% and 75%) on the characterizations of compressed bacterial cellulose nanopaper film. The film was prepared with different heat treatments; compression at 25 °C for 72 h and then at 100 °C for 24, 72 or 120 h. Maximum tensile strength (250.7 MPa) and tensile modulus (18.6 GPa) were measured on the film treated at 100 °C for 120 h and RH 50%. However, tensile strength and tensile modulus dropped by 53.6% and 75.8% respectively and elongation at break increased by 32% when this film was stored in more humid conditions (RH 75%). FTIR spectra and XRD patterns indicate changes of the deformed chain structure of the cellulose as more water was incorporated between the layers of the lattice after exposure to humidity.

* Corresponding author.
E-mail address: habral@yahoo.com (H. Abral).
https://doi.org/10.1016/j.jmrt.2021.01.057

1. Introduction

Cellulose is the most abundant organic compound in nature and is synthesized by a variety of microorganisms such as bacteria, algae and fungi [1]. Bacterial cellulose (BC) is secreted directly as nanofibres by cellulose-producing bacteria to form a pellicle (e.g. a thick bio-film) floating on top of a static fermentation medium [2]. BC is a pure biopolymer, without collateral biogenic compounds like lignin, hemicelluloses, or pectin [3]. The BC pellicle nanofibers form a porous tridimensional network of cross-linked fibers immersed in a liquid matrix [4]. Unlike many natural fibers, the BC can be used in the production of nanopaper without the use of corrosive chemicals [2,5]. The mechanical and electrical properties of the nanopaper are known to vary with water content [6]. However, stable tensile and physical properties of hydrophilic cellulose-based nanopaper regardless of humidity would be an asset in many industrial applications.

Compression is a common mechanical method in the preparation of cellulose nanopaper [7–9]. Research has shown that compression of BC mats at 100 MPa at 70 °C increased in the tensile strength of about 182 MPa [9]. Cellulose film is hydrophilic attracting water molecules which diffuse between through the cellulose intra- and interchains. The presence of these water molecules may promote relaxation of the lattice strain resulting in the cellulose chains becoming more mobile. Many previous works have explored the effect of humidity on the mechanical and physical properties of cellulose-based materials [10–13]. The mechanical properties of cellulose nanocrystal film have been found to decrease with increasing humidity [10]. However, the role of humidity of the lattice structure in the decrease of tensile properties remains unclear. FTIR and XRD have been considered the effective tools to study the change of cellulose molecular structure [14]. This paper employs these technologies (FTIR and XRD) to study the effects of two different levels of humidity on the characterizations of the crystalline structure of compressed bacterial cellulose nanopaper film.

2. Materials and methods

2.1. Materials

Wet BC pellicle cuboids (250 mm × 150 mm × 25 mm) were purchased from the same home industry in Padang, Indonesia that manufactures in the form of *nata de coco* used in our previous work [4]. The original pellicle which was purified using distilled water and analytical grade sodium hydroxide (Brataco Brand), and adsorbent (silica gel) was supplied by the Andeska Laboratory and PT. Brataco, Padang, Indonesia.

2.2. Preparation of sample

The *nata de coco* pellicle was cleaned with distilled water until pH 7 then cut into rectangles (50 mm × 100 mm) with a steel knife. The purified pellicle was soaked in 5% NaOH for 24 h and rinsed repeatedly with distilled water until pH 7. The wet pellicle was clamped using a stainless steel flange which was compressed using a hydraulic press at a pressure of 8 MPa for 3 days at 25 °C to form an unheated film (labeled as 0 h). Other clamped pellicles (8 MPa) were stored in a drying oven (Memmert UN-55) at 100 °C for 24, 72 or 120 h to produce heated films (labeled as 24 h, 72 h or 120 h, respectively). All unheated and heated films were peeled off the flange and directly stored in a desiccator chamber with relative humidity (RH) of 50% or 75% at 25 °C for 3 days. The RH level of the chamber was controlled using adsorbent sodium silicate (Na_2SiO_3) at $\leq$ 2% RH, and measured by a humidity meter (HTC-1, Hebei, China).

2.3. Characterization

2.3.1. Morphology investigation using field emission scanning electron microscopy (FESEM)

The FESEM samples were placed on the FESEM sample stub. All samples were coated with carbon followed by gold for 2 min using an argon plasma metallizer (sputter coater K575X) (Edwards Limited, Crawley, United Kingdom) to reduce the electron charge. A field-emission scanning electron microscope FEI Nova NanoSEM 230 (FEI, Brno-Černovice, Czech Republic) was used with 10 kV at 20,000x magnification to optimize observation of the surface morphology of the sample and the fracture surface of the tensile sample was observed.

2.3.2. Tensile properties

A Com–Ten testing machine 95 T was used to measure tensile properties (tensile strength (TS), tensile modulus (TM), and elongation at break (EB)) performed with a tensile speed of 5 mm/min at room temperature. ASTM D638-type V is the standard used for tensile testing and all samples were cut to 63.5 mm length and 9.5 mm width [15]. Before testing, all samples were conditioned for 48 h at 50 ± 5% relative humidity and 25 °C in a desiccator. Thickness and width of the film were measured using a dial micrometre to 1 μm accuracy. Tensile tests were repeated five times for each sample.

2.3.3. FTIR

Prior to FTIR characterization, dried samples were stored in a closed chamber with RH 50% or 75% for 24 h. FTIR of the sample was characterized using a PerkinElmer Frontier equipment. The film was scanned at a frequency range of 4000–600 cm^{-1} at 4 cm^{-1} resolution.

2.3.4. XRD testing

The crystallinity index (I_{cr}) can be quantified using XRD method [16]. Dried samples were stored in a closed chamber with RH 50% or 75% for 24 h before XRD characterization. X-ray diffraction testing was carried out using PANalytical Xpert PRO at 25 °C, 40 kV and 30 mA. The samples were scanned from $2\theta = 5^{\circ}$ to 50° with $\lambda = 0.154$ nm. Percentage of I_{cr} was measured using Eq. (1) [17]:

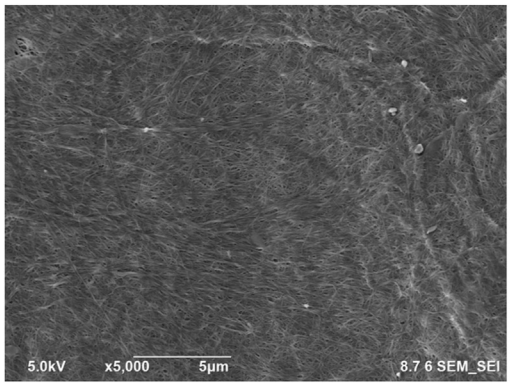
5.0kV x5,000 5μm 8.7 6 SEM_SEI

a.

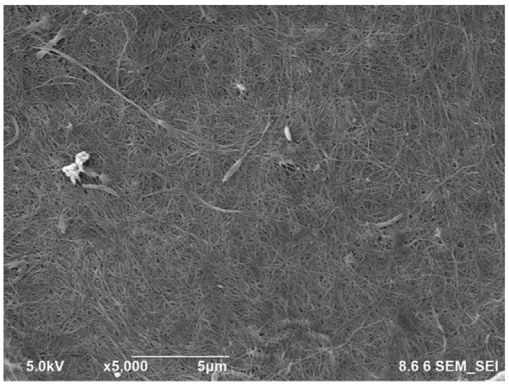
5.0kV x5,000 5μm 8.6 6 SEM_SEI

b.

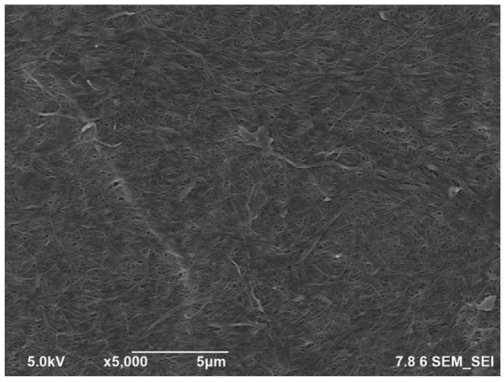
5.0kV x5,000 5μm 7.8 6 SEM_SEI

c.

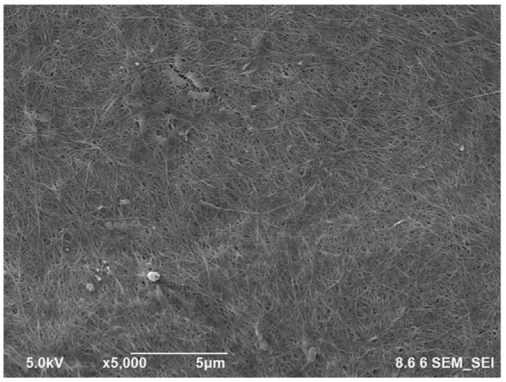
5.0kV x5,000 5μm 8.6 6 SEM_SEI

d.

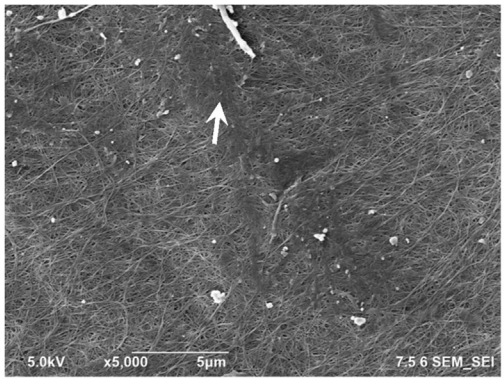
5.0kV x5,000 5μm 7.5 6 SEM_SEI

e.

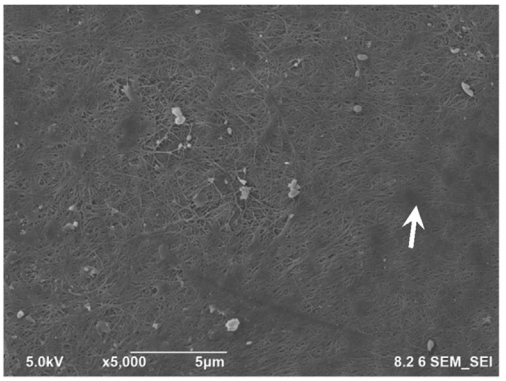
5.0kV x5,000 5μm 8.2 6 SEM_SEI

f.

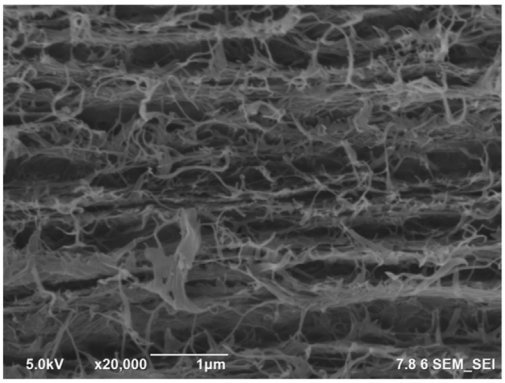
5.0kV x20,000 1μm 7.8 6 SEM_SEI

g.

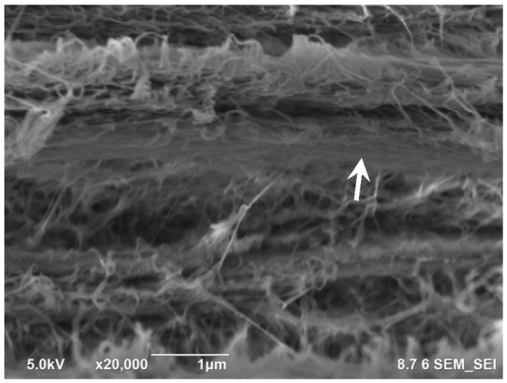
5.0kV x20,000 1μm 8.7 6 SEM_SEI

h.

$$I_{cr}\ (\%) = \frac{(I_{200} - I_{am})}{I_{200}} \times 100 \quad (1)$$

where I_{200} is the maximum intensity of the peak corresponding to cellulose I, and I_{am} is the minimum intensity of the amorphous fraction between the 101 and 200 peak.

2.3.5. *Statistical analysis*

Experimental data were analyzed using IBM SPSS Statistics 25.0 (IBM Corporation, Chicago, USA). One-way analysis of variance (ANOVA) and p-test were used to identify the significance of any effects of dry and humid conditions (RH 50% and 75%) on tensile properties of the nanopaper film.

3. Results and discussion

3.1. *FESEM morphology*

Fig. 1 shows the FESEM morphology of the BC nanopaper film for each treatment. The appearance of the film surfaces at RH 50% (Fig. 1a, c) or 75% (Fig. 1b, d) was similar; humidity did not obviously change the appearance of the films. Longer compression duration at 100 °C increased in compactness of the nanofiber (marked with a white arrow in Fig. 1e, f). A similar phenomenon was also observed on the fracture surface of the compressed film which was heated at 100 °C for 120 h and shows more fractions of high nanofiber density (marked with a white arrow in Fig. 1h) in comparison to the compressed film treated at 25 °C for 120 h (Fig. 1g). This denser nanofiber section has greater interconnection between the cellulose molecules on the surface through hydrogen bonding. The highly interconnected nanofibers have low mobility which can obstruct the movement of mobile nanofibers. Consequently, more fractions of the low nanofiber mobility may increase tensile strength and modulus, and decrease elongation at break of the BC film (see Fig. 4). In contrast to Fig. 1h, g shows a fracture surface with a larger number of big cavities, and less compact network structure. Therefore, the cellulose chain as shown in Fig. 1g was more mobile than that in Fig. 1h. Consequently, BC nanopaper with the mobile nanofiber had low tensile strength and modulus but its elongation at break was high.

3.2. *FTIR spectra*

The effect of treatment on the functional groups of the cellulose can be observed using FTIR spectroscopy [18]. Fig. 2a and b displays FTIR for each sample averaged from triplicate measurements. All spectra display a similar pattern, however, there are differences in the broadness, intensity and wavenumber value of the peak (see Fig. 2c-k for more details). The main peaks at about 3310, 2897, 1640, 1328 and 1030 cm^{-1} correspond to O–H stretching (Fig. 2c), C–H stretching (Fig. 2d-e), O–H bending (Fig. 2f-g), C–C and C–O skeletal vibrations (Fig. 2h-i), and C–O stretching (Fig. 2j-k) respectively [19–22]. The wavenumbers of O–H stretching shifted to a higher value (see Table 1) as humidity increased. This is attributable to the hydrogen bond interaction between the O–H groups of cellulose and water [23]. The shape of the band at RH 50% was broader as a result of the more disoriented crystal (Fig. 2c). This shape became sharper at higher humidity (RH 75%). A similar phenomenon is also observed for other functional groups (Fig. 2d-i). The increased sharpness of the band for the hydroxyl groups was attributed to an increase in intra- and intermolecular hydrogen bonds and chain reordering [23,24]. This explanation is supported by the ratio value between the absorbance bands at 3324/1320 cm^{-1} (see Table 1) demonstrating the increased hydrogen bonding [25]. A similar trend was also presented by the wavenumber of about 1640 cm^{-1} (Fig. 2f-g) showing lower value at lower humidity. This phenomenon is similar to previous work that the absorption maximum of the water peak shifts slightly toward a higher wavenumber as the relative humidity increases [23]. The peak intensity at 1640 cm^{-1} for BC sample exposed to RH 50% decreased as heating duration increased (Fig. 2f) due to water evaporation [26]. In contrast, the intensity at this band (1640 cm^{-1}) for BC exposed to RH 75% shows a different trend (Fig. 2g). The 24 h and 72 h samples had a stronger peak intensity than the 0 h sample. The hydroxyl groups in the cellulose polymer can reform hydrogen bonds between different cellulose polymers or within the polymer itself [27]. The intramolecular bonds give stiffness to the polymer chain, while the intermolecular bonds allow the linear polymers to reform sheet structures [28]. Intermolecular bond formation leads to an increase in the rigidity of the cellulose chain network resulting from an increase in the structural relaxation. However, after longer heating durations the peak intensity became weaker indicating a decrease in hydrophilic nature and probably an increase in the amount of the aggregated crystalline cellulose microfibrils which are less hydrophilic than nonaggregated microfibrils.

Table 1 – The crystallinity index (I_{cr}) from Fig. 3 (without normalization), the hydrogen bond intensity (HBI) at A3338/A1330 cm^{-1} from Fig. 2, O–H stretching vibration wavenumber (cm^{-1}) and transmittance (T %) for samples at RH 50% or 75% from Fig. 2.

Sample	RH (%)	I_{cr} (%)	HBI	OH-Stretching	
				3340 cm^{-1}	T %
0 h	50	89.34	1.9	3337	18.46
24 h		88.63	2.0	3339	17.83
72 h		87.66	2.0	3338	28.12
120 h		91.45	2.1	3340	26.12
0 h	75	85.44	2.1	3339	23.19
24 h		90.93	2.1	3340	19.51
72 h		91.12	2.2	3342	23.51
120 h		91.26	2.0	3345	25.87

Fig. 1 – FESEM morphology of nanopaper film prepared with various treatments. Surface of film treated at 25 °C for 72 h and RH 50% (a) or RH 75% (b); Surface of film treated at 100 °C for 24 h at RH 50% (c) or RH 75% (d); for 72 h (e) or 120 h (f) at RH 50%; from fracture surface at 25 °C for 72 h and RH 50% (g) or at 100 °C for 120 h at RH 75% (h).

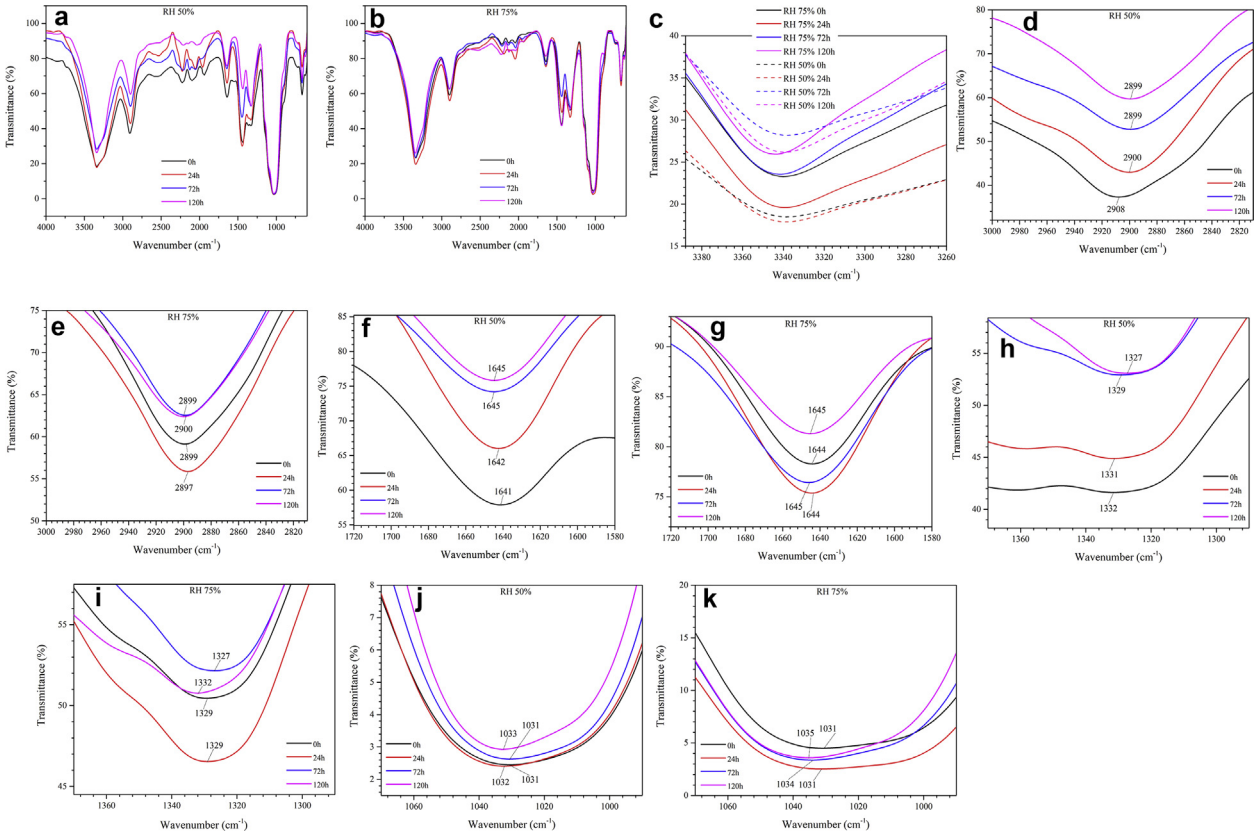

Fig. 2 – FTIR spectra of BC nanopaper films formed with different heating durations at 100 °C (a–b) The full spectrum from 4000 to 250 cm^{-1} (c–k) sections of the spectrum expanded to show changes in peaks related to specific functional groups after storage in a closed chamber with RH 50% or RH 75%.

The peaks at wavenumber 1290-1390 cm^{-1} at RH 50% (Fig. 2h) were broad probably corresponding to a highly disoriented crystal structure [24]. After RH 75% exposure (Fig. 2i) the peak became sharper which can be related to the reduction of lattice strain [29–31]. The band at about 1030 cm^{-1} corresponding to C–O stretching is related to the backbone structure of cellulose [32]. The 0 h films for both RH 50% and 75% showed peaks at the lowest wavenumber at 1029 cm^{-1} and 1031 cm^{-1} respectively. These bands at RH 75% (Fig. 2k) were sharper than that at RH 50% (Fig. 2j). Wavenumber position at RH 75% shifted from 1031 cm^{-1} (0 h film) to 1035 cm^{-1} (120 h film). This shifting was more visible than in the RH 50% film. The reason for the 0 h films has the lowest wavenumber and the broadest band is because the cellulose structure was probably experiencing the strongest deformation [33,34]. This deformation causes an increase in the microfibril density, a decrease in the bond lengths and the interlayer spacing of chains, consequently a decrease in the vibration of the deformed molecules. These cellulose networks in higher humidity interact with more water molecules creating intra- and intermolecular hydrogen bonds [27]. Consequently, the cellulose structures expand and molecular chains move into more thermodynamically favourable positions. This phenomenon results in an increase in the molecular vibration recorded in FTIR spectra as a shift to a higher wavenumber value. These results reconfirm that the cellulose film with higher deformation of cellulose structures was more relaxed and had a higher sensitivity to higher humidity.

3.3. *XRD pattern*

Fig. 3 displays XRD patterns of samples exposed to 50% or 75% RH. The main peaks were observed at about $2\theta = 14.5°$ and $2\theta = 22.5°$ corresponding to the (101) and (200) crystal plane which indicates a semi-crystalline nature [35]. This is characteristic of pure bacterial cellulose [4]. Compression results in a decrease in the peak intensity and a broadening of the peaks as shown by Fig. 3a and b without normalization (i). Table 1 displays the crystallinity index (I_{cr}) of each sample as a function of heating duration for various RH. I_{cr} value overall increases as temperature increases. The X-ray diffraction profile, notably at RH 75%, presents narrower and sharper peaks as a result of an increase in the crystallinity of the structures (see inset of Fig. 3b). This suggests that absorption of water molecules into the structure did not decrease in the I_{cr} value but did increase the crystal spacing. When the

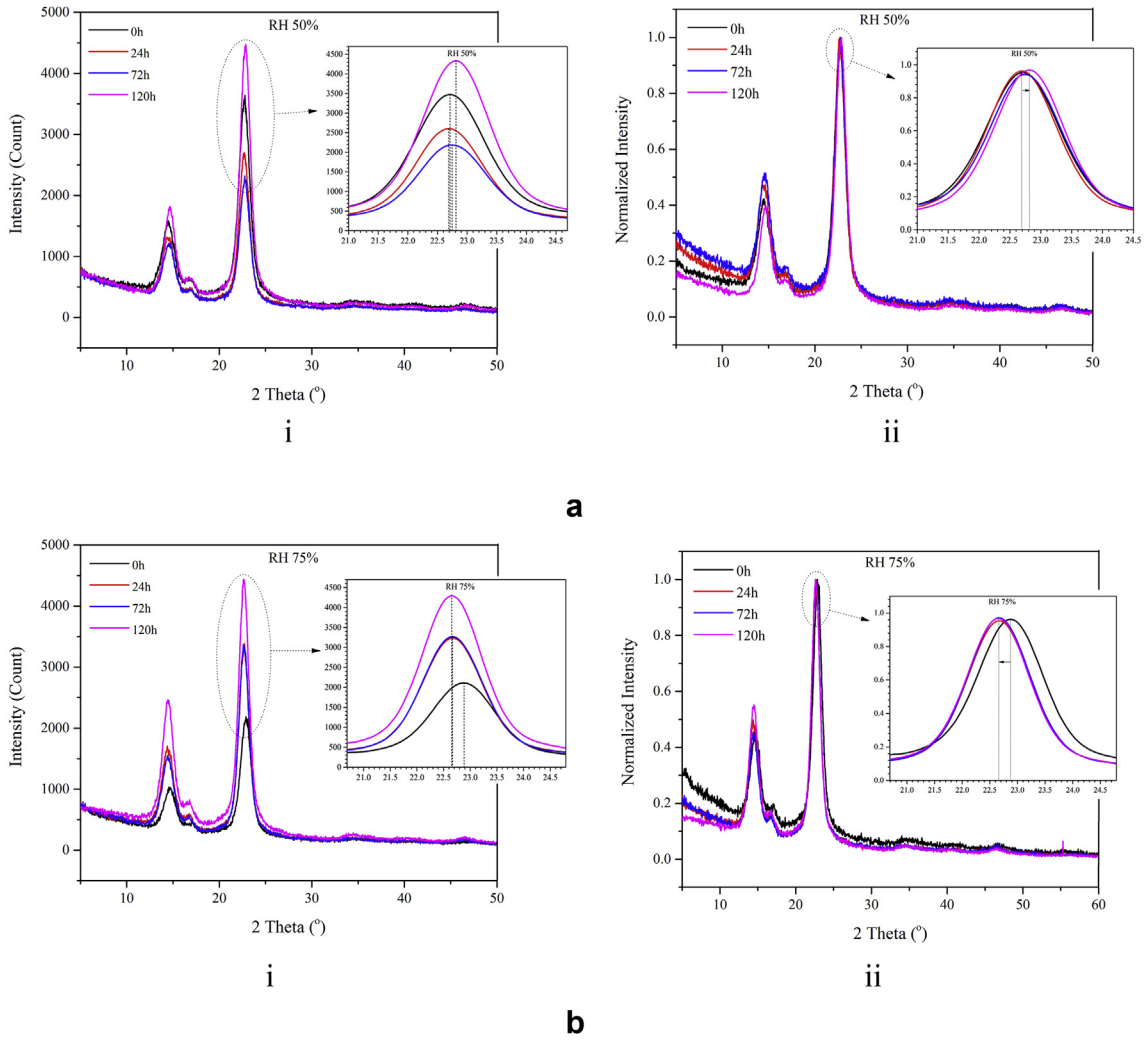

Fig. 3 – XRD curves of nanopaper with RH 50% (a) and 75% (b) without (i) and with normalization (ii).

material is under stress, the interlayer spacing of cellulose chains can increase or decrease, which leads to a shift in the peak positions in an XRD pattern [36].

According to previous research, a shift the peak position to the right side after compression (see normalized XRD curve of Fig. 3a(ii)) can be associated with an increase in compressive residual stress resulting from a decrease in the interlayer spacing of the cellulose polymer chains [36–38]. The peak position for the unheated nanopaper film (0 h film) at RH 50% was $2\theta = 22.7°$ lower than the same film after exposure to 75% RH ($2\theta = 22.9°$) probably due to different lattice spacing [38]. This peak (200 plane) position for the 120 min heated nanopaper after storing in RH 50% was still at a larger angle than that of the unheated film. This is because the increase in absorbed water molecules at this degree of humidity was not sufficient to restructure the lattice plane. In contrast, RH 75% exposure caused the peak to shift toward the left side or to smaller angles for all samples (see normalized XRD curve of Fig. 3b(ii)) showing an expansion of lattice planes as a result of the presence of more water molecules relaxing the chain structures and releasing activation energy [38]. A slight increase in the bound water was measured on the ratio between the absorbance bands at 3400 and 1320 cm^{-1} at RH 75% compared to RH 50% [39].

3.4. *Tensile properties*

Fig. 4 shows TS (a), TM (b), and EB (c) of cellulose film after exposure to RH 50% or 75%. After further heating, TS and TM increased and EB decreased. An increase in these properties was obviously in the RH 50% attributed to decreased degree of molecular chain mobility resulting from the denser chain network, greater amount of the interconnected nanofibers, and the presence of the compressive residual stress. The external tensile stress must overcome the compressive residual stress before the crack tips experiences sufficient tensile stress to propagate. Maximum TS (250.7 MPa) and TM (18.6 GPa) were measured in the film treated at 100 °C for 72 h after RH 50% exposure (246% and 597% increases compared to the nontreated film). In this case, TS improved by 116%

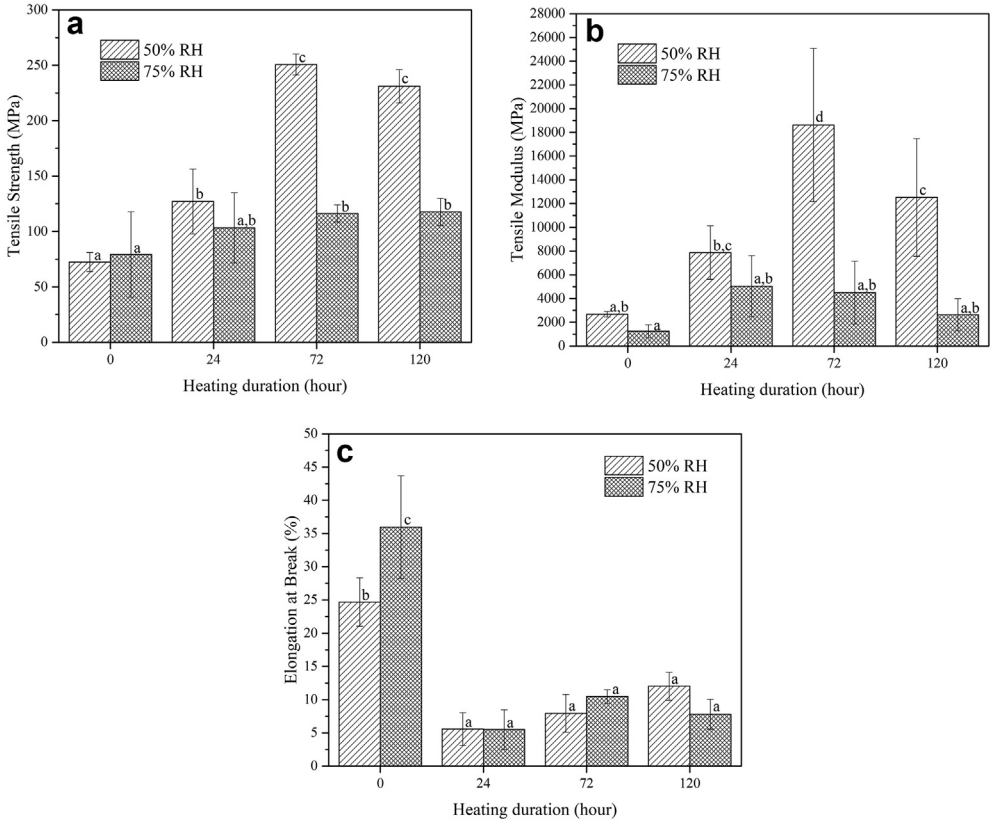

Fig. 4 – TS (a), TM (b) and EB (c) for unheated and heated samples.

compared to the same film exposed to RH 75%. However, the value of TS dropped from 250.7 MPa to 116.2 MPa (a decrease by 53.6%) at this humidity and surprisingly EB increased after the film was stored in a more humid room. This probably corresponds to a decrease in compressive residual stress resulting from relaxation of the cellulose chain structure which was promoted by more water molecules. This result is in agreement with Fig. 3b (XRD pattern) showing more relaxation for samples stored in higher humidity (RH 75%). The incorporation of more water molecules at RH 75% restructured chain networks via inter- and intramolecular hydrogen bonds leading to an increase in the interlayer spacing and the length of the bonds, thus an increase in the cellulose chain mobility. Significantly more mobile chain structures were observed in unheated (0 h) film which had a higher elongation at break at RH 75% (EB = 36%) than 50% (EB = 25%).

4. Conclusion

Tensile properties of compressed BC film were found to be strongly dependent on the humidity level and the presence of the residual stress. Longer heating duration increased tensile strength and the tensile modulus of the film particularly when under conditions of lower humidity (RH 50%). This increase corresponds to lower cellulose chain mobility due to a denser network structure of the nanofibril and higher compressive residual stress. This internal stress opposes external tensile stress increasing the TS and TM. However, exposure to higher humidity (RH 75%) resulted in a relaxation of the lattice planes, thus reducing the compressive residual stress. Consequently, TS and TM dropped and the stiffness of the film decreased.

Declaration of Competing Interest

The authors declare no conflict of interest.

Acknowledgement

Acknowledgement is addressed to Universitas Andalas for supporting research funding with project name Riset Publikasi Guru Besar, number T/5/UN.16.17/PP.IS-KRP1GB/LPPM/2020.

REFERENCES

[1] Satari B, Karimi K, Kumar R. In: Cellulose solvent-based pretreatment for enhanced second-generation biofuel production: a review, vol. 3. Royal Society of Chemistry; 2019. https://doi.org/10.1039/c8se00287h.

[2] Hervy M, Blaker JJ, Braz AL, Lee KY. Mechanical response of multi-layer bacterial cellulose nanopaper reinforced polylactide laminated composites. Compos Part A Appl Sci Manuf 2018;107:155–63. https://doi.org/10.1016/j.compositesa.2017.12.025.
[3] Tischer PCSF, Sierakowski MR, Westfahl H, Tischer CA. Nanostructural reorganization of bacterial cellulose by ultrasonic treatment. Biomacromolecules 2010;11:1217–24.
[4] Abral H, Lawrensius V, Handayani D, Sugiarti E. Preparation of nano-sized particles from bacterial cellulose using ultrasonication and their characterization. Carbohydr Polym 2018;191:161–7.
[5] Abral H, Hartono A, Hafizulhaq F, Handayani D, Sugiarti E, Pradipta O. Characterization of PVA/cassava starch biocomposites fabricated with and without sonication using bacterial cellulose fiber loadings. Carbohydr Polym 2018;206:593–601. https://doi.org/10.1016/j.carbpol.2018.11.054.
[6] Rebelo A R, Archer AJ, Chen X, Liu C, Yang G, Liu Y. Dehydration of bacterial cellulose and the water content effects on its viscoelastic and electrochemical properties. Sci Technol Adv Mater 2018;19:203–11. https://doi.org/10.1080/14686996.2018.1430981.
[7] Henriksson M, Berglund LA, Isaksson P, Lindström T, Nishino T. Cellulose nanopaper structures of high toughness. Biomacromolecules 2008;9:1579–85. https://doi.org/10.1021/bm800038n.
[8] Hu L, Zheng G, Yao J, Liu N, Weil B, Eskilsson M, et al. Transparent and conductive paper from nanocellulose fibers. Energy Environ Sci 2013;6:513–8. https://doi.org/10.1039/c2ee23635d.
[9] Retegi A, Gabilondo N, Peña C, Zuluaga R, Castro C, Gañan P, et al. Bacterial cellulose films with controlled microstructure-mechanical property relationships. Cellulose 2010;17:661–9. https://doi.org/10.1007/s10570-009-9389-7.
[10] Wu Q, Meng Y, Concha K, Wang S, Li Y, Ma L, et al. Influence of temperature and humidity on nano-mechanical properties of cellulose nanocrystal films made from switchgrass and cotton. Ind Crop Prod 2013;48:28–35. https://doi.org/10.1016/j.indcrop.2013.03.032.
[11] Gennadios A, Park HJ, Weller CL. Relative humidity and temperature effects on tensile strength of edible protein and cellulose ether films. Trans ASAE 1993;36:1867–72. https://doi.org/10.13031/2013.28535.
[12] Yousefi H, Faezipour M, Hedjazi S, Mousavi MM, Azusa Y, Heidari AH. Comparative study of paper and nanopaper properties prepared from bacterial cellulose nanofibers and fibers/ground cellulose nanofibers of canola straw. Ind Crop Prod 2013;43:732–7. https://doi.org/10.1016/j.indcrop.2012.08.030.
[13] Ebrahimzadeh PR, Kubát DG. Effects of humidity changes on damping and stress relaxation in wood. J Mater Sci 1993;28:5668–74. https://doi.org/10.1007/BF00367845.
[14] Dai D, Fan M. Investigation of the dislocation of natural fibres by Fourier-transform infrared spectroscopy. Vib Spectrosc 2011;55:300–6. https://doi.org/10.1016/j.vibspec.2010.12.009.
[15] ASTM D882 - 12. Standard test method for tensile properties of thin plastic sheeting. Am Soc Test Mater 2002.
[16] Ju X, Bowden M, Brown EE, Zhang X. An improved X-ray diffraction method for cellulose crystallinity measurement. Carbohydr Polym 2015;123:476–81. https://doi.org/10.1016/j.carbpol.2014.12.071.
[17] Segal L, Creely JJ, Martin AE, Conrad M. Empirical method for estimating the degree of crystallinity of native cellulose using the X-ray diffractometer. Textil Res J 1958:786–94.
[18] Kolar J, Strlič M, Marinček M. IR pulsed laser light interaction with soiled cellulose and paper. Appl Phys Mater Sci Process 2002;75:673–6. https://doi.org/10.1007/s003390201309.
[19] Syafri E, Kasim A, Abral H, Sudirman, Sulungbudi GT, Sanjay MR, et al. Synthesis and characterization of cellulose nanofibers (CNF) ramie reinforced cassava starch hybrid composites. Int J Biol Macromol 2018;120:578–86. https://doi.org/10.1016/j.ijbiomac.2018.08.134.
[20] Nacos MK, Katapodis P, Pappas C, Daferera D, Tarantilis PA, Christakopoulos P, et al. Kenaf xylan - a source of biologically active acidic oligosaccharides. Carbohydr Polym 2006;66:126–34. https://doi.org/10.1016/j.carbpol.2006.02.032.
[21] Sun XF, Xu F, Sun RC, Fowler P, Baird MS. Characteristics of degraded cellulose obtained from steam-exploded wheat straw. Carbohydr Res 2005;340:97–106. https://doi.org/10.1016/j.carres.2004.10.022.
[22] Abral H, Ariksa J, Mahardika M, Handayani D, Aminah I, Sandrawati N, et al. Transparent and antimicrobial cellulose film from ginger nanofiber. Food Hydrocoll 2020;98:105266. https://doi.org/10.1016/j.foodhyd.2019.105266.
[23] Velazquez G, Herrera-Gómez A, Martín-Polo MO. Identification of bound water through infrared spectroscopy in methylcellulose. J Food Eng 2003;59:79–84. https://doi.org/10.1016/S0260-8774(02)00428-4.
[24] Abral H, Ariksa J, Mahardika M, Handayani D, Aminah I, Sandrawati N, et al. Effect of heat treatment on thermal resistance, transparency and antimicrobial activity of sonicated ginger cellulose film. Carbohydr Polym 2020;240:116287. https://doi.org/10.1016/j.carbpol.2020.116287.
[25] Oh SY, Dong IY, Shin Y, Hwan CK, Hak YK, Yong SC, et al. Crystalline structure analysis of cellulose treated with sodium hydroxide and carbon dioxide by means of X-ray diffraction and FTIR spectroscopy. Carbohydr Res 2005;340:2376–91. https://doi.org/10.1016/j.carres.2005.08.007.
[26] Cheng D, Li T, Smith G, Yang J, Hang C, Miao Z, et al. Influence of calcium chloride impregnation on the thermal and high-temperature carbonization properties of bamboo fiber. PLoS One 2019;14:1–12. https://doi.org/10.1371/journal.pone.0212886.
[27] Chami Khazraji A, Robert S. Self-assembly and intermolecular forces when cellulose and water interact using molecular modeling. J Nanomater 2013;2013:1–12. https://doi.org/10.1155/2013/745979.
[28] Börjesson M, Westman G. Crystalline nanocellulose — preparation, modification, and properties. Intech; 2016. p. 13. https://doi.org/10.5772/57353.
[29] Chalmers JM, Mackenzie MW, Willis HA, Edwards HGM, Lees JS, Long DA. FTIR spectroscopic studies of isotactic polypropylene films under stress. Spectrochim Acta Part A Mol Spectrosc 1991;47:1677–83. https://doi.org/10.1016/0584-8539(91)80005-4.
[30] Svenson MN, Thirion LM, Youngman RE, Mauro JC, Bauchy M, Rzoska SJ, et al. Effects of thermal and pressure histories on the chemical strengthening of sodium aluminosilicate glass. Front Mater 2016;3:1–11. https://doi.org/10.3389/fmats.2016.00014.
[31] Brown EN, Clausen B, Brown DW. In situ measurement of crystalline lattice strains in phase IV polytetrafluoroethylene. J Neutron Res 2007;15:131–8. https://doi.org/10.1080/10238160701372620.
[32] Wiley JH, Atalla RH. Band assignments in the Raman spectra of celluloses. Carbohydr Res 1987;160:113–29. https://doi.org/10.1016/0008-6215(87)80306-3.

[33] Tanpichai S, Quero F, Nogi M, Yano H, Young RJ, Lindström T, et al. Effective young's modulus of bacterial and microfibrillated cellulose fibrils in fibrous networks. Biomacromolecules 2012;13:1340–9. https://doi.org/10.1021/bm300042t.

[34] Kačuráková M, Smith AC, Gidley MJ, Wilson RH. Molecular interactions in bacterial cellulose composites studied by 1D FT-IR and dynamic 2D FT-IR spectroscopy. Carbohydr Res 2002;337:1145–53. https://doi.org/10.1016/S0008-6215(02)00102-7.

[35] Tsouko E, Kourmentza C, Ladakis D, Kopsahelis N, Mandala I, Papanikolaou S, et al. Bacterial cellulose production from industrial waste and by-product streams. Int J Mol Sci 2015;16:14832–49. https://doi.org/10.3390/ijms160714832.

[36] Epp J. X-ray diffraction (XRD) techniques for materials characterization. Elsevier Ltd; 2016. https://doi.org/10.1016/B978-0-08-100040-3.00004-3.

[37] Bandyopadhyay R, Selbo J, Amidon GE, Hawley M. Application of powder X-ray diffraction in studying the compaction behavior of bulk pharmaceutical powders. J Pharm Sci 2005;94:2520–30. https://doi.org/10.1002/jps.20415.

[38] Cao W, Ma C, Tan S, Ma M, Wan P, Chen F. Ultrathin and flexible CNTs/MXene/cellulose nanofibrils composite paper for electromagnetic interference shielding. Nano-Micro Lett 2019;11:1–17. https://doi.org/10.1007/s40820-019-0304-y.

[39] Poletto M, Ornaghi Júnior HL, Zattera AJ. Native cellulose: structure, characterization and thermal properties. Materials (Basel) 2014;7:6105–19. https://doi.org/10.3390/ma7096105.